Ozone deposition measurements over wheat fields in the North China Plain: variability and related factors of deposition flux and velocity

Xiaoyi Zhang[1,2], Wanyun Xu[1, *], Weili Lin[3], Gen Zhang[1], Jinjian Geng[4,5], Li Zhou[4,5], Huarong Zhao[4,5], Sanxue Ren[4,5], Guangsheng Zhou[4,5], Jianmin Chen[2] and Xiaobin Xu[1, *]

[1] State Key Laboratory of Severe Weather, Key Laboratory for Atmospheric Chemistry, Institute of Atmospheric Composition, Chinese Academy of Meteorological Sciences, Beijing, China, 100081

[2] Department of Atmospheric and Oceanic Sciences, Fudan University, Shanghai, China, 200433

[3] College of Life and Environmental Sciences, Minzu University of China, Beijing, China, 100081

[4] State Key Laboratory of Severe Weather, Institute of Agricultural Meteorology, Chinese Academy of Meteorological Sciences, Beijing, China, 100081

[5] Hebei Gucheng Agricultural Meteorology National Observation and Research Station, Baoding, China, 072656

Correspondence to: Wanyun Xu (xuwy@cma.gov.cn) and Xiaobin Xu (xiaobin_xu@189.cn)

Abstract. Ozone (O_3) deposition is the main sink of surface O_3, exerting great influences on air quality and ecosystem. Due to instrument limitations and method shortages, O_3 deposition was less observed and investigated in China, where O_3 has been reported to be on continuous and significant rise. Here, we conducted comprehensive measurements of O_3 deposition over wheat canopy at a typical polluted agricultural site in the North China Plain using a newly developed relaxed eddy accumulation system. For the main wheat growing season in 2023, O_3 deposition flux and velocity (V_d) averaged -0.25 ± 0.39 µg m^{-2} s^{-1} and 0.29 ± 0.33 cm s^{-1}, respectively. Daytime V_d (0.40 ± 0.38 cm s^{-1}) was obviously higher than in the nighttime (0.17 ± 0.26 cm s^{-1}). The temporal changes of V_d were mainly determined by crop growth, and V_d significantly increased with decreasing relative humidity, and increasing friction velocity and soil water content, enhanced by higher leaf area index. With rapid increases of soil moisture, simultaneous and following overall increments in V_d were detected, attributed to remarkably strengthening O_3 stomatal uptake under increased stomatal conductance and extended opening to the night, and more non-stomatal O_3 removal at night resulted from strengthened soil NO emission at moist conditions. This study confirms the leading effects of crop growth on O_3 deposition modulated by environmental conditions and the non-negligible influences of nocturnal plant activities, and emphasizes the needs for O_3 deposition observation over different surfaces and accurate evaluation of O_3 agricultural impacts based on deposition fluxes.

1 Introduction

Surface ozone (O_3) is a key secondary air pollutant, generated in photochemical reactions involving volatile organic compounds (VOCs), nitrogen oxides (NO_x = NO ＋NO_2) (Seinfeld et al., 2006). Over the past two decades, China's rapid economic development and increasing anthropogenic emissions of NO_x and VOCs have led to significantly upward trends in O_3 concentrations (Monks et al., 2015; Li et al., 2019; Lu et al., 2020; Xu et al., 2020), especially in the North China Plain

(NCP) (Tai et al., 2014; Ma et al., 2016; Wang et al., 2017; Lu et al., 2020; Xu, 2021; Wang et al., 2022; Lyu et al., 2023). Dry deposition plays one of the key roles in removing surface O_3 (e.g., (Tang et al., 2017) and contributes about 20% to the annual global tropospheric O_3 loss (Lelieveld and Dentener, 2000; Wild, 2007; Hardacre et al., 2015). Over vegetated areas, stomatal and non-stomatal uptake of O_3 may represent major part of the total dry deposition (Fowler et al., 2001). Plant uptake of large amount of O_3 may cause a series of deleterious oxidative reactions, damaging vegetation and threatening crop quality and production (Ainsworth, 2017; Harmens et al., 2018; Mills et al., 2018; Feng et al., 2019b). In addition, O_3 deposition to the ground surfaces (including soil, snow and water) is closely related to tropospheric chemistry, air quality and ecosystems (Clifton et al., 2020a; Stella et al., 2019; Helmig et al., 2012; Stocker et al., 1995). Under the rapid expansion of population and growing demands for food, China has become the largest crop producer, as well as importer (Dong et al., 2021). O_3 deposition is thus of great importance and its accurate quantification is urgently needed to evaluate the impact of increasing O_3 levels on agricultural production, ecosystem, air quality, human health, and global climate.

O_3 deposition has been measured over various ecosystems, including forest, grassland, cropland and bare soil environments (Table S1), in order to understand deposition mechanisms and evaluate its potential effects (Stella et al., 2019; Xu et al., 2018; Zhu et al., 2015; Helmig et al., 2012; Mészáros et al., 2009; Lamaud et al., 2009; Coyle et al., 2009). However, the deposition processes are controlled by various biotic (stomatal uptake) and abiotic (non-stomatal removal) activities that are simultaneously modulated by environmental factors. The relative contributions of stomatal and non-stomatal O_3 deposition varied with land cover, plant species and growth stages, as well as environmental factors. Stomatal uptake of O_3 depends on the opening and closure of stomata on leaf surfaces. For example, the fraction of diurnal maximum stomatal O_3 deposition over boreal forests ranged from 56 to 74% (Rannik et al., 2012), while only accounting for 31.2% in a wheat field (Xu et al., 2018), with both of them peaking at mid-day during the most rigorous growth stage of vegetations (Xu et al., 2018; Rannik et al., 2012). Non-stomatal resistance of O_3 decreased with the increasing temperature and friction velocity, and was ~ 50% lower under wet conditions than under dry conditions over the same potato canopy (Coyle et al., 2009). Thus, O_3 deposition is dominated by distinct deposition processes over different surfaces in different environments.

Currently, the eddy covariance (EC) method and flux-gradient (FG) approach are the most commonly used micrometeorological techniques for measuring O_3 vertical fluxes (Businger and Oncley, 1990; Altimir et al., 2006; Wu et al., 2015; Clifton et al., 2020b). However, EC requires robust fast-response measurement instruments ($\geq$ 10 Hz) (Hicks and Wesely, 1978; Muller et al., 2009), while the assumption of FG is dependent on surface roughness and the photochemical reactions of O_3 and its precursors (Raupach and Thom, 1981; Vilà-Guerau De Arellano and Duynkerke, 1992). These relatively high requirements have more or less limited the application of traditional micrometeorological methods to the measurements of O_3 flux. The relaxed eddy accumulation (REA) method is another important micrometeorological method for observing the air-surface exchange of interested substances over ecosystems (Desjardins, 1977; Businger and Oncley, 1990). REA overcomes the need for fast-response gas sensors, and is based on the same physical principle as EC without introducing other uncertainties (Pattey et al., 1993). REA relies on the conditional sampling of air at a constant flow rate according to the instantaneous vertical velocity, which requires high-response sampling valves (~ 10 Hz). The air samples associated with

updrafts and downdrafts are accumulated into two separate reservoirs and accurately measured with slow-response gas analyzers (Businger and Oncley, 1990). In addition, REA sampling systems are of low-cost, easily portable and simple to operate, which allows easy deployment at remote locations in forests, over croplands and grassland surfaces (Sarkar et al., 2020). Thus, REA methods have been widely applied in flux measurements of various species, such as biogenic VOCs (Mochizuki et al., 2014), reduced sulfur gases (Xu et al., 2002), HONO (Ren et al., 2011) and aerosols (Matsuda et al., 2015; Xu et al., 2021) above forest canopies, peroxyacetyl nitrate at a grassland site (Moravek et al., 2014) , NH_3 above fertilized corn (Nelson et al., 2017) and Hg at an urban site and over a boreal peatland (Osterwalder et al., 2016). To the best of our knowledge, the REA method has not been applied in O_3 deposition flux measurements so far.

Although many regions in China have been experiencing severe O_3 pollution during growing seasons, measurements of O_3 flux over crop fields in the country have only been sporadically reported, which were made using either chamber techniques (e.g., Tong et al., 2015) or micrometeorological approaches (Zhu et al., 2014; Zhu et al., 2015; Xu et al., 2018). In this study, we developed a new REA flux system and applied it to obtain O_3 deposition fluxes over wheat fields in the NCP during the springtime growing season. Based on these in-situ observations, we evaluated the feasibility of O_3 flux measurements using the REA method, analyzed the variation characteristics of O_3 deposition during the wheat growing season, identified the key drivers in the variability of daytime and nighttime O_3 deposition during distinct crop growth stages and different environmental conditions, respectively.

2 Observation and method

2.1 Site description

The flux observations were conducted at the Gucheng site (39°08'N, 115°40'E, GC), an integrated ecological-meteorological observation and research station of the Chinese Academy of Meteorological Science, located 35 km to the northeast of urban Baoding City, Hebei Province, and 100 km southwest to urban Beijing. The site is surrounded mainly by irrigated high-yield agricultural lands with small villages, and a highway connecting Beijing and Shijiazhuang 7 km to the west of the site (Figure S1). The fields within and surrounding the yard of GC are on a winter wheat-summer maize rotation, which is typical in Northern China. Observations at the site have revealed good regional representativeness of the agricultural areas in the NCP, that is heavily impacted by the severe regional air pollution (Lin et al., 2009; Xu et al., 2019; Kuang et al., 2020; Zhang et al., 2022a, b).

2.2 Relaxed eddy accumulation (REA) technique

2.2.1 Theory

A self-assembled relaxed eddy accumulation system for O_3 dry deposition measurements (REA-O_3 flux system) was deployed at GC. In the REA-O_3 flux system, conditional sampling is conducted according to the direction of vertical wind (w),

which separates sampled air into updraft and downdraft reservoirs at a constant flow rate (Desjardins, 1977; Businger and Oncley, 1990). The vertical fluxes of O_3 (F_{O_3}, in $\mu g\ m^{-2}\ s^{-1}$) are calculated by the concentration differences between two reservoirs following Eq. (1):

$$F_{O_3} = \overline{w'\ c'} = b\sigma_w\left(\overline{c^+} - \overline{c^=}\right), \qquad \text{Eq. (1)}$$

where σ_w is the standard deviation of vertical wind (in $m\ s^{-1}$); $\overline{c^+}$ and $\overline{c^=}$ are the averaged O_3 concentrations in the updraft and downdraft reservoirs, respectively (in $\mu g\ m^{-3}$); b is the eddy accumulation coefficient and is obtained from CO_2 flux measured using the EC method and calculated using Eq. (2):

$$b = \frac{\overline{w'CO_2'}}{\sigma_w\left(\overline{CO_2^+} - \overline{CO_2^=}\right)}, \qquad \text{Eq. (2)}$$

where $\overline{CO_2^+}$ and $\overline{CO_2^=}$ are averaged CO_2 concentration observed under upward and downward vertical winds, respectively (in $mg\ m^{-3}$), $\overline{w'CO_2'}$ represents the EC CO_2 flux (in $mg\ m^{-2}\ s^{-1}$). Based on the measurements from February to June 2023, b revealed an average $\pm$ standard deviation of 0.55 ± 0.09, ranging from 0.16 to 0.80.

O_3 deposition velocity (V_d, $cm\ s^{-1}$) is estimated based on O_3 flux and concentrations using Eq. (3):

$$V_d = -\frac{F_{O_3}}{C_{O_3}} \times 100, \qquad \text{Eq. (3)}$$

where C_{O_3} is the 30 min averaged O_3 concentration (in $\mu g\ m^{-3}$).

2.2.2 System setup and verification

The setup of the REA-O_3 flux system is depicted in Figure 1. A 3-D sonic anemometer (CSAT3, Campbell Scientific Inc., USA) was used for measuring the three wind components (u, v, w) at 10 Hz, which was amounted at the height of 4.5 m on an eddy covariance tower, located in the middle of cropland. The height of the flux tower was designed according to the result of the fetch and footprint analysis. The range of flux source region was about 400 m, which is covered by the crop field within the GC station. The inlet (1/8" OD Teflon tubing) of the REA system was installed in the center of the anemometer. The 10 Hz wind signals, together with the signals from the CO_2/H_2O analyzer (Li-7500, LI-COR, Inc., USA), were collected by a datalogger (CR1000, Campbell Scientific Inc., USA) and sent to a PC. The wind signals were processed by a program written in Python, which also sent switch command to two fast-response 3-way solenoid valves (LVM105R-5C, Sintered Metal Company, Japan) according to the vertical wind direction. Based on the direction of instantaneous vertical winds, sample air was drawn alternatively through updraft or downdraft sample tubes (1/4" OD Teflon) wrapped in aluminum foil and were analyzed by the two UV photometric O_3 analyzers (TE 49i, Thermo Fisher Scientific Inc., USA) installed at the ends of updraft and downdraft channels, respectively. Coarse particulate matter was filtered out of air samples using two particle filters (47 mm single stage filter assembly, Savillex, LCC., USA) before entering the O_3 analyzers (Figure 1). To ensure the stability of airflow in the O_3 analyzers and sampling system, zero air was supplied to the channel that was not sampling ambient air. The zero air was generated by an external air compressor (M104, Gast Manufacturing Inc., USA) and a zero-air generator (Model 111, Thermo Fisher Scientific Inc., USA), which removes O_3, NO, NO_2, CO and hydrocarbons from ambient air, but not water

vapor. In addition, both sampling tubes were bypassed through a piston pump (617CD22, Gardner Denver Thomas Inc., USA), in order to increase the inlet sample flow and avoid the axial mixing before the solenoid valves. The linear velocity of air sample in the inlet tubing was set to 22 m s^{-1}, and airflow was at the turbulent state with a Reynolds number over 2300. The

130   estimated residence time from system inlet to the valves was 18 ms, while the response time of the fast-response sampling valves was less than 10 ms, leading to total time delays from inlet to individual sampling tubes of below 10 ms, thus the REA system could work at a sample frequency of 10 Hz (100 ms). Total residence time of air samples from the tip of the inlet to the point of O_3 detection was about 10 s, which was much shorter that the lifetime of O_3 reacting with NO (Supplementary methods), suggesting the chemical reaction in the two channels could be neglected. The O_3 analyzers recorded 1-minute

135   averaged O_3 concentrations, which were downloaded by the PC. O_3 data were synchronized with wind data as well as sample time according to the PC time. The actual averaged O_3 concentrations under updraft and downdraft conditions were calculated according to Eq. (4) using the sample time, sample flow and 1-minute averaged O_3 concentrations:

$$\bar{c} = \frac{\sum_{i=1}^{i=30} c_i \times flow_i}{\sum_{i=1}^{i=30} flow_i \times t_{sample\ gas,i}},$$ Eq. (4)

where c_i is the 1-minute averaged O_3 concentration (in µg m^{-3}), $flow_i$ is the 1-minute averaged sample flow (in SLPM)

140   measured by the mass flow meter (MFM), and $t_{sample\ gas,i}$ is the real time for analyzing air sample within ith minute (in fraction of a minute). The O_3 concentration was calculated by averaging O_3 concentrations under updraft and downdraft conditions using Eq. (5).
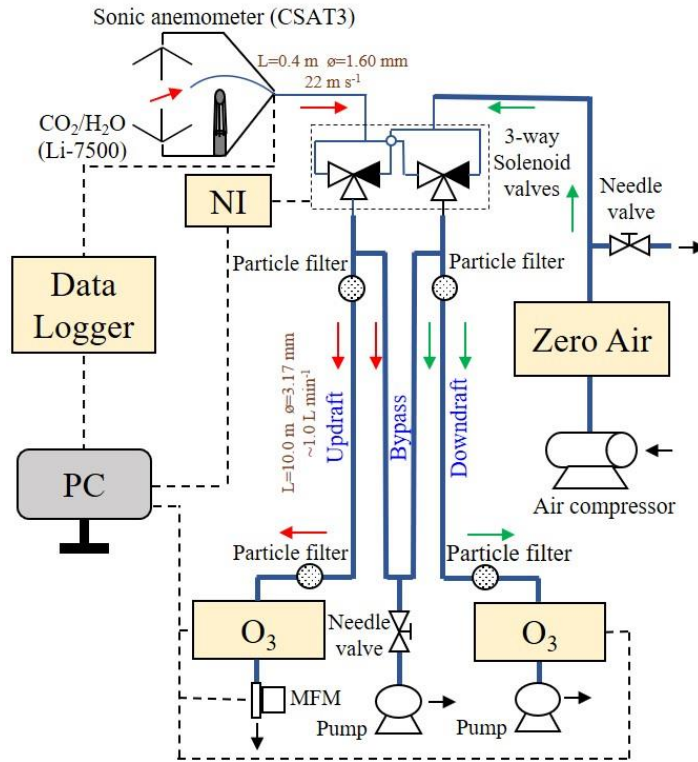
$$C_{O_3} = \frac{\overline{c^+} + \overline{c^-}}{2}$$ Eq. (5)

Figure 1. Schematic of the REA-O_3 flux system ($w > w_0$).

To increase the concentration difference between updraft and downdraft, a wind speed threshold called the wind dead-band (w_0) was used in the REA system to discard air samples associated with w close to 0. The application of w_0 promotes the sampling of larger eddies that contribute more to gas fluxes. If a proper w_0 is used, the eddy frequency spectrum shifts to the low frequencies in the sample, but does not cut off all the high-frequency signals, only filtering out samples with small vertical displacements that have relatively small impacts on the overall flux (Bowling et al., 1999; Held et al., 2008; Tsai et al., 2012; Moravek et al., 2014; Grelle and Keck, 2021). Conditional sampling using w_0 also prolongs the lifetime of the fast-response solenoid valves (Pattey et al., 1993) and effectively avoids sampling error around $w = 0$ due to the limitation of the sonic anemometer (Grelle and Keck, 2021). In the REA-O_3 system, we adopted fixed wind dead-bands during the daytime (from 08:00 to 18:00 Local Time (LT), $w_0 = 0.05$ m s^{-1}) and night (from 19:00 to 07:00 LT, $w_0 = 0.01$ m s^{-1}), respectively, considering that wind speeds during the daytime were generally larger than those at night. The concentration difference increased with w_0 and led to an increase in measured fluxes. Using raw EC data, the REA CO_2, H_2O and heat fluxes were calculated under w_0 in this study (0.05 m s^{-1} for daytime and 0.01 m s^{-1} for nighttime) and $w_0 = 0$, respectively, with a constant b of 0.60 (Businger and Oncley, 1990). As shown in Figure S2, the two flux datasets revealed excellent correlations during the whole observation period, with a correlation coefficient close to 1, confirming the reliability and stability of the REA flux measurement system. Compared with the fluxes without w_0, CO_2, H_2O and heat fluxes with w_0 exhibited similar small overestimations, reaching

around 10-13% during the daytime and 4-10% at night, which were comparable with the influence of a dynamic dead-band ($w_0 = \frac{\sigma_w}{0.35}$) in Grelle and Keck's (2021) REA system for H_2O, CO_2, CH_4, N_2O flux measurements. This indicates that adopting the wind dead-band in our REA system only had marginal impact on observed fluxes.

To identify potential flux errors induced by any differences between updraft and downdraft channels in the REA-O_3 system (including valves, sample tubes and O_3 analyzers), the parallelism of the two sampling channels was checked through simultaneous direct sampling of ambient O_3 from the REA system inlet during 10-11 May. As shown in Figure S3, O_3 data points obtained from the two channels all aligned close to the 1:1 line (slope = 1.02, p < 0.01), suggesting that the difference in measured O_3 was minimal between updraft and downdraft reservoirs and that its impact on flux measurement could be ignored. Moreover, synchronous multipoint calibrations of the two channels were conducted monthly. Different O_3 concentrations generated by an O_3 calibrator (TE 49C PS, Thermo Fisher Scientific Inc., USA) were introduced into the system from the zero air inlet and simultaneously measured by the two O_3 analyzers. Figure S4 presents the results of multipoint calibration, with determination coefficients (R^2) reaching 1.000, indicating high stability of the two channels and O_3 instruments. O_3 concentrations in the two channels were adjusted based on the results of parallel experiments and standard calibrations.

To further verify the reliability of the REA system, the flux data derived from the REA technique with those based on the EC theory. For CO_2, H_2O and heat, the averaged ratios of REA to EC fluxes were all slightly larger than 1, indicating small overestimates in the REA flux measurement system, which were expected due to the use of w_0. Most of the flux data maintained high consistency with correlation coefficients close to 1 (Figure S5), confirming that the REA system performed reliably under most conditions.

2.3 Field measurements and ancillary data

Measurements of O_3 flux were conducted during the main wheat growing season in 2023, from the late of dormancy stage (13 February 2023) to wheat harvest (18 June 2023). According to the winter wheat phenology at GC (Table S1), its entire growth season could be divided into three stages: Over-Wintering (O-W, 13 February-5 March), Green-Flowering (G-F, 6 March-28 May) and Ripening-Harvest (R-H, 29 May-18 June). The wheat height increased from 6.0 cm during the O-W stage to 61.2 cm at the R-H stage. Ancillary data were obtained for further analysis, including meteorology data, soil parameters, plant growth indicators and O_3 related trace gas measurement data. Meteorological variables including air temperature (T_{Air}), relative humidity (RH), precipitation, soil temperature (T_{Soil}) and volumetric water content (soil VWC) at 20 cm, global solar radiation (G), photosynthetic active radiation (PAR) and sun elevation angle were measured by an automatic weather station at GC. The 30 min CO_2, H_2O, heat and momentum fluxes were measured by the EC system, which includes a 3-D sonic anemometer, an open path CO_2/H_2O analyzer and a datalogger. The friction velocity (u_*) was calculated using the three wind components (u, v, w) following Eq. (6), and the vapor pressure deficit (VPD) was estimated as in Eq. (7).

$$u_* = \left(\overline{u'w'}^2 + \overline{v'w'}^2 \right)^{1/4} ,$$
Eq. (6)

$$VPD = (1 - \frac{RH}{100}) \times 611.2 \times exp(\frac{17.62 \times T_{Air}}{243.12 + T_{Air}}) \div 100 \ ,$$ Eq. (7)

The Leaf Area Index (LAI) and the Fraction of Photosynthetically Active Radiation (FPAR) were obtained from the Moderate Resolution Imaging Spectroradiometer (MODIS) Level 4 product (MCD15A3H) with a spatial resolution of 500 m and temporal resolution of 4 days (Myneni et al., 2015).

NO_x ($NO/NO_2/NO_x$) concentrations were monitored from 18 March to 2 June by a NO-NO_2-NO_x Trace Level Analyzer (Model 42C-TL, Thermo Fisher Scientific Inc., USA). The analyzer is installed in an air-conditioned container on the northern edge of the cropland, which is located 200 m north of the eddy covariance tower. The air inlet is 1.8 m above the roof of the container and ~ 4.5 m above ground level, with an estimated residence time of less than 3 s. Multipoint calibrations of NO_x were made using a NO standard gas obtained from National Institute of Metrology, Beijing, China. A total set of 3631 30-min averaged NO_x data were obtained, as shown in Figure S6. During the measurement period, NO concentration ranged from 0.1 ppb to 23.3 ppb with an average of 0.8 ± 1.8 ppb, while NO_2 ranged from 0.5 ppb to 6.6 ppb with an overall average of 2.3 ± 0.9 ppb.

2.4 Stepwise multiple linear regression (MLR) model

Stepwise multiple linear regression (MLR) models were applied to identify the key environmental factors influencing O_3 deposition in the daytime (sun elevation angle > 0°) and nighttime (sun elevation angle < 0°), respectively. MLR is a commonly used approach to describe the relationship between air pollution and its influencing factors (Zhang et al., 2022b; Han et al., 2020; Fu and Tai, 2015; Rannik et al., 2012). The stepwise MLR model takes the following form:

$$y = \beta_0 + \sum_{k=1}^{n} \beta_k x_k \ ,$$ Eq. (8)

where y is the observed V_d, x_k is the selected normalized environmental parameter, β_0 is the regression constant, β_k is the regression coefficient and n is the number of selected term. β_k is determined by a forward stepwise method to add and delete terms to obtain the best model fit based on Akaike Information Criterion (AIC) statistics (Venables and Ripley, 2003). The Z-Score normalization method was adopted according to the following equation:

$$x = (x_{observed} - x_{mean}) \div x_{standard\ deviation} \ ,$$ Eq. (9)

where $x_{observed}$, x_{mean} and $x_{standard\ deviation}$ are the observed parameters, its overall average and standard deviation, respectively. Environmental parameters including seven meteorological and soil factors (T_{Air}, RH, VPD, u_*, T_{Soil}, soil VWC and PAR) and two crop related factors (LAI, FPAR) were considered during daytime, while PAR was unaccounted for during nighttime. The selected variables in the stepwise MLR were considered to be the environmental factors critical for O_3 deposition at GC during the wheat growing season.

3 Results and discussion

3.1 Meteorological conditions

Figure 2 shows the temporal variations of daily meteorological and soil conditions during the whole period. Air and soil temperatures gradually increased from the lowest values (T_{Air}: -0.8 °C, T_{Soil}: 2.9 °C) in February to highest ones (T_{Air}: 30.2 °C, T_{Soil}: 30.9 °C) in June. RH varied around a higher level before the latter part of April and a lower level after that, with an average of 64 ± 17 %. Calculated u_* fluctuated in the range of 0.05-0.30 m s^{-1}, with an average of 0.17 ± 0.04 m s^{-1}. Daily VPD was relatively stable during February-early April, with an average of 5.9 ± 4.0 hPa., and rose obviously afterwards, reaching an averaged value of 19.9 ± 7.4 hPa during May to June. During the wheat growth stage, the cropland experienced two irrigation events, occurring on 19-21 April and 18-22 May, respectively (Figure 2c). The irrigation system mainly consists of an irrigation pump with the outlet flow of 50 m^3 h and a total of 20 sprinklers. The total irrigation water volume was approximately 3600 m^3 for 3333 m^2 cropland, and the duration was 3 days. Soil VWC kept flat before the middle of April and showed dramatical boosts caused by strong precipitation or irrigation events during 9-10, 20-21, 28-29 April and 19-20 May (Figure 2c), followed by slow declines due to evapotranspiration under higher temperatures. Both PAR and G exhibited great fluctuations with slight increases from February to June.
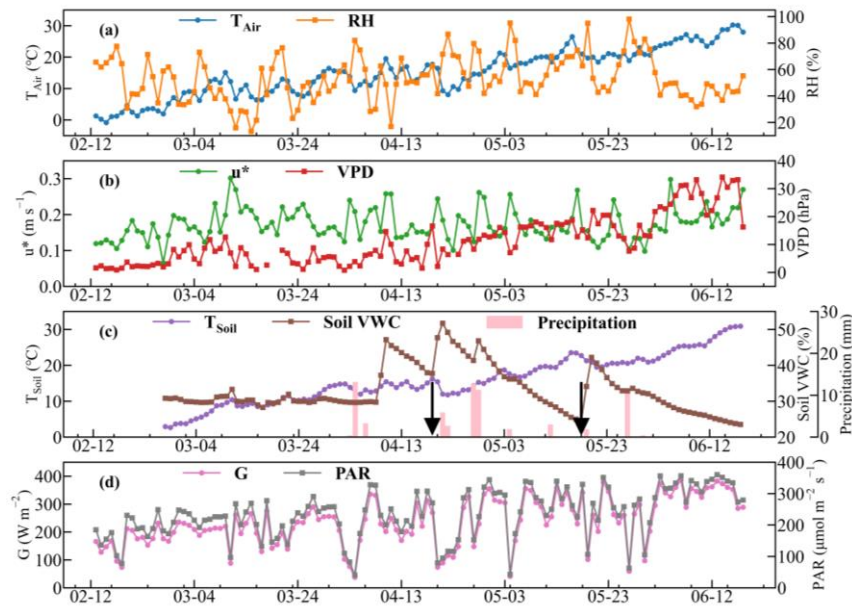
Figure 2. Daily meteorological and soil conditions from 12 February to 18 June 2023: (a) T_{Air} and RH, (b) u_* and VPD, (c) irrigation (black arrows), precipitation, T_{Soil} and soil VWC, (d) G and PAR.

3.2 O₃ flux, deposition and concentration

Totally 2728 pairs of O₃ deposition flux and velocity were obtained for the wheat growing season, which are presented in Figure 3, along with 30-min and daily average O₃ concentrations. O₃ deposition flux averaged -0.25 ± 0.39 μg m^{-2} s^{-1}, with a larger deposition during daytime (-0.39 ± 0.45 μg m^{-2} s^{-1}) and a smaller one during nighttime (-0.08 ± 0.21 μg m^{-2} s^{-1}). The largest negative (-3.20 μg m^{-2} s^{-1}) and positive (0.14 μg m^{-2} s^{-1}) fluxes were measured during noontime on 29 April and during midnight on 15 March, respectively. Daytime V_d averaged 0.40 ± 0.38 cm s^{-1} and was distinctly higher than nighttime ones (0.17 ± 0.26 cm s^{-1}). The averages of daytime and nighttime V_d obtained in this study were comparable to those from previous EC-based observations (0.42 cm s^{-1} and 0.14 cm s^{-1}) during the wheat growing season and higher than those (0.29 cm s^{-1} and 0.09 cm s^{-1}) during the maize growing season (Table S2) in Shangdong Province, China (Zhu et al., 2015; Zhu et al., 2014). V_d averaged 0.29 ± 0.33 cm s^{-1} over the whole observation period, ranging from -0.39 cm s^{-1} to 2.65 cm s^{-1}. The average O₃ deposition velocities observed over the wheat canopy did not show substantial differences from those previously reported for grasslands (Mészáros et al., 2009; Coyle, 2005), forests (Wu et al., 2015; Rannik et al., 2012) and bare soil (Stella et al., 2019) (Table S2). O₃ concentrations over the wheat canopy were significantly enhanced after April, with an overall average of 61.8 ± 34.6 μg m^{-3}. In general, O₃ deposition velocities were more pronounced from mid-April to late-May (Figure 3b), when wheat was growing vigorously, while deposition fluxes were higher after late May due to overall higher O₃ concentration (Figure 3a, c). Thus, O₃ concentration was more determinative of O₃ deposition flux than V_d on longer timescales.
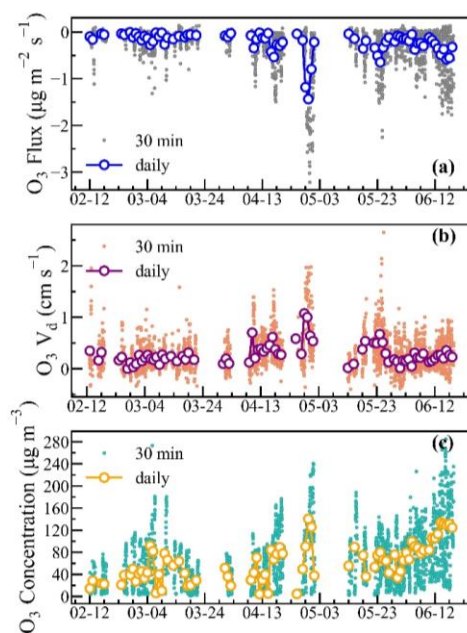
Figure 3. Timeseries of O₃ deposition flux (a), V_d (b) and concentration (c) during the wheat growing season.

The averaged diurnal patterns of O_3 deposition flux, velocity and O_3 concentration are depicted in Figure 4. With solar radiation and atmospheric turbulence increasing after sunrise, plant stomatal conductance increased along with H_2O, CO_2 fluxes over the cropland, reaching peaks at noon (Figure 5). O_3 deposition rapidly rose during the morning (06:00-10:00). Deposition flux and velocity both reached their peaks (-0.62 μg m^{-2} s^{-1} and 0.54 cm s^{-1}) by 13:00, when stomatal conductance and gas-leaf exchange also reached the diurnal maximums (Rannik et al., 2012; Otu-Larbi et al., 2021). O_3 deposition quickly decreased from 14:00 to 18:00 despite of high levels of O_3 (Figure 4). At night, atmospheric turbulence weakened and leaf stomatal closed, resulting in reduced H_2O and CO_2 fluxes keeping steady throughout the night (Figure 5). Nighttime O_3 deposition remained at relatively low levels and exhibited weak changes, with an averaged flux and V_d of -0.09 ± 0.04 μg m^{-2} s^{-1} and 0.17 ± 0.02 cm s^{-1}, respectively. Therefore, diel variations in O_3 deposition over the wheat fields were mainly driven by the stomatal opening and closing, with O_3 deposition velocity being decisive of deposition flux diurnal variations.
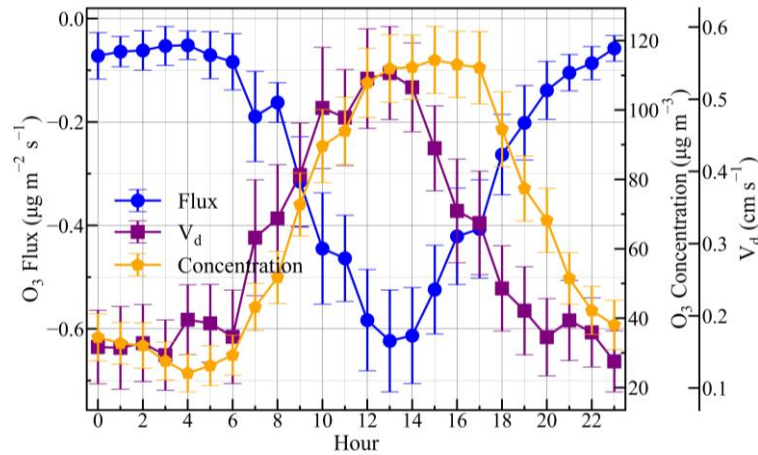
Figure 4. Diurnal variations of O_3 deposition flux, V_d and concentration during the wheat growing season, with error bars representing average ± 0.2 × standard deviation values.

3.3 O_3 deposition in different stages of wheat growth

To investigate the influences of wheat growth on O_3 deposition, the characteristics of O_3 deposition were further examined in connection to the different growth stages. During the O-W stage, wheat was in dormancy and leaves had not begun to turn green (LAI < 0.5, Figure 6b), with CO_2 flux in the agricultural ecosystem closed to zero (Figure 6c). V_d in the O-W stage barely changed, exhibiting a low average value of 0.20 ± 0.28 cm s^{-1} and a median of 0.12 cm s^{-1} (Table 1). Wheat grew vigorously in the G-F stage, with LAI and CO_2 assimilation flux exhibiting rapid increases until the early and late flowering stage, respectively, after which both of them gradually decreased (Figure 6b-c). O_3 deposition varied nearly in synchronization with LAI and wheat growth, with V_d reaching a peak when cropland CO_2 assimilation was the highest during the G-F stage (Figure 6a), reaching highest daytime and nighttime averages of 0.46 ± 0.41 cm s^{-1} and 0.24 ± 0.28 cm s^{-1}, respectively (Table 1). Afterwards, with the maturing of wheat and the aging of leaves in the R-H stage, V_d quickly dropped back to a low average level of 0.20 ± 0.25 cm s^{-1}, similar to that observed in the O-W stage. It can be seen that the temporal variation of O_3 deposition velocity over wheat was predominantly determined by crop growth at GC. As for the deposition flux, both the daily and daytime averaged fluxes during the G-F stage were comparable with those in the R-H stage (Table 1), which can be attributed to the high O_3 concentrations in the summer months (Zhang et al., 2022a; Lin et al., 2009). Although nighttime O_3 concentration during the G-F stage was also 58% lower than that in the R-H stage, nighttime O_3 deposition flux during the G-F stage was still the highest among the three stages, which was related to the remarkably high nighttime deposition velocities during the G-F stage (Table 1).
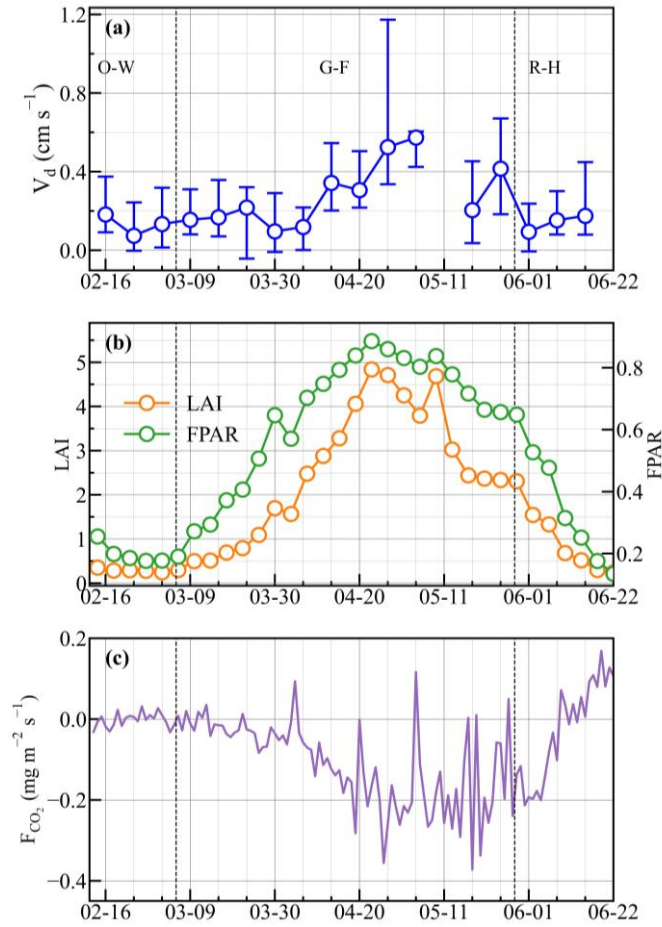
Figure 6. (a) O_3 V_d, (b) LAI and FPAR, (c) CO_2 flux (F_{CO_2}) in different wheat growing stages. The circles and error bars in (a) denote the weekly medians and quantiles of V_d, respectively. O-W, G-F and R-H represent Over-Wintering, Green-Flowering and Ripening-Harvest stages.

Table 1. Summary of daily, daytime and nighttime O_3 V_d and flux during the O-W, G-F and R-H stages.

		Over-Wintering			Green-Flowering			Ripening-Harvest		
		All	Day	Night	All	Day	Night	All	Day	Night
V_d	Mean	0.20	0.29	0.12	0.36	0.46	0.24	0.20	0.30	0.05
(cm s^{-1})	Standard Deviation	0.28	0.30	0.24	0.37	0.41	0.28	0.25	0.26	0.14
	Median	0.12	0.24	0.07	0.28	0.38	0.17	0.15	0.26	0.07
	75%	0.33	0.39	0.22	0.51	0.61	0.37	0.33	0.48	0.13
	25%	0.01	0.11	-0.02	0.11	0.20	0.06	0.05	0.12	-0.01

O$_3$ flux (μg m^{-2} s^{-1})									
Mean	-0.10	-0.19	-0.02	-0.28	-0.42	-0.12	-0.27	-0.40	-0.06
Standard Deviation	0.18	0.22	0.06	0.45	0.51	0.27	0.37	0.41	0.12
Median	-0.03	-0.11	-0.01	-0.10	-0.26	-0.02	-0.12	-0.27	-0.04
75%	0.00	-0.03	0.00	-0.01	-0.08	-0.01	-0.02	-0.08	0.00
25%	-0.11	-0.28	-0.03	-0.36	-0.53	-0.10	-0.40	-0.62	-0.09

3.4 O$_3$ deposition relation to environmental factors

To gain deeper insights into the responses of O$_3$ deposition (including stomatal and non-stomatal) to environmental factors in agricultural areas, stepwise MLR models were conducted to see which factors potentially played more important roles in O$_3$ deposition at GC during daytime and nighttime, respectively. As shown in Table 2, RH, u$_*$, soil VWC and LAI were identified as significant environmental factors in explaining daytime O$_3$ deposition changes during the entire observation period. Additionally, the coefficients of determination (R^2) of the linear model between all environmental factors and V$_d$ was 0.46, implying that these meteorological and plant growth related factors could explain approximately 46% of the variance of daytime O$_3$ deposition, while R^2 was only slightly lower (0.43) with the four selected factors. Distinct key environmental factors for O$_3$ deposition were identified for different wheat growth stages, while LAI was only among the most important factors during the G-F stage (Table 2), confirming the significant effect of crops on O$_3$ deposition during its most vigorous growing stage. During the O-W stage, wheat played a minor role in O$_3$ deposition as LAI < 0.5. Solar radiation (PAR) and wind (u$_*$) supplied energy for atmospheric turbulence, which transported O$_3$ to soil surface, while soil moisture (soil VWC) largely affected the diffusion and absorption of O$_3$ in soil (Stella et al., 2011a). Therefore, O$_3$ deposition was more sensitive to u$_*$, soil VWC and PAR during the O-W stage. In the R-H stage, the land surface was covered by ripe wheat, which reduced LAI and stomatal conductance. O$_3$ deposition was therefore mainly dependent on turbulent transport, which was more affected by T$_{Air}$ and u$_*$ under sufficient solar radiation (Fig. 2d). During nighttime, O$_3$ deposition mainly commenced through non-stomatal pathways such as cuticular and soil deposition (Xu et al., 2018), that are affected by turbulence strength and surface condition. The most significant influencing factors for O$_3$ deposition were T$_{Air}$, u$_*$, T$_{Soil}$ and soil VWC for the whole observation period (Table 2). However, temperatures (T$_{Air}$ and T$_{Soil}$) were not selected as the key factors when the stepwise MLR was separately done for the three growth stages. Compared with the R^2 of daytime MLR model, meteorological and soil conditions could explain more variance of the nighttime O$_3$ deposition (54%), implying that nighttime O$_3$ deposition processes were less complicated than daytime ones.

Table 2. Results of the MLR models for the O-W, G-F and R-H stages. Daytime MLR models represent multiple linear regression between daily average environmental variables and daytime O$_3$ V$_d$, while nighttime models represent nighttime environmental variables and V$_d$. The selected MLR models refer to the stepwise MLR model based on AIC statistics. Bold numbers denote those with p-value < 0.05.

	Whole Period			Over-Wintering			Green-Flowering			Ripening-Harvest		
	MLR	Selected MLR		MLR	Selected MLR		MLR	Selected MLR		MLR	Selected MLR	
	Coef.	Coef.	Std. Err.	Coef.	Coef.	Std. Err.	Coef.	Coef.	Std. Err.	Coef.	Coef.	Std. Err.
					Daytime							
T_{Air}	-0.09			0.13			-0.08			0.01	**0.09**	**0.02**
RH	-0.08	**-0.06**	**0.03**	0.04			-0.07	-0.08	0.04	0.07		
u_*	0.04	0.05	0.03	0.04	**0.09**	**0.02**	0.08	0.08	0.04	-0.07	**-0.06**	**0.02**
VPD	-0.06			-0.05			-0.09			0.11		
T_{Soil}	0.11			0.00			0.24			-0.21		
soil VWC	0.10	**0.10**	**0.04**	-0.01	-0.05	0.02	0.14	0.07	0.06	-0.36		
PAR	0.01			0.04	-0.04	0.04	0.05			0.03		
LAI	0.19	0.07	0.05	-0.06			0.30	0.08	0.06	0.60		
FPAR	-0.14			-0.05			-0.34			-0.45		
R^2	0.46	0.43		0.93			0.53	0.47		0.64	0.56	
					Nighttime							
T_{Air}	-0.24	**-0.20**	**0.08**	0.05			-0.15			0.12		
RH	-0.07			0.08			-0.11			-0.08	-0.03	0.02
u_*	0.02	**0.03**	**0.02**	-0.07			-0.01			0.02	**0.03**	**0.02**
VPD	-0.01			0.08			-0.02			-0.11		
T_{Soil}	0.20	**0.18**	**0.06**	0.20			0.12			-0.11		
soil VWC	0.12	**0.12**	**0.02**	0.15	**0.07**	**0.02**	0.11	**0.12**	**0.02**	-0.10	-0.03	0.02
R^2	0.54	0.49		0.99	0.71		0.57	0.39		0.58	0.52	

Further, we explored how the selected key factors controlled the temporal variability of V_d during the three wheat growth stages (Figures 7-9). In general, the responses of both daytime and nighttime V_d to the meteorological factors were consistent throughout the entire wheat growth season (Figures 7 and 9).

Ambient RH influences the relative contributions of stomatal and non-stomatal processes to O_3 deposition. A clear negative variation of V_d with increasing RH was observed at GC both for daytime and nighttime (Figure 7a and 9b). Due to the negative correlation of VPD to RH (Eq.7), high VPD was conducive to high nighttime V_d (Figure 9c). During daytime, this negative relationship was detected for all growth stages, while during nighttime the decrease with RH was most evident during the G-F stage. At RH above 60-70%, leaf surfaces are frequently covered by a thin liquid film or by dew water, which would inhibit stomatal dry deposition, but enhance aqueous reactions of O_3, leading to enhanced relative contribution of non-stomatal deposition, however, with high variability (Coyle et al., 2009; Lamaud et al., 2009). Under RH below 60%, stomatal

conductance contributes more to O_3 deposition, which might also be negatively dependent on RH. For instance, similar negative correlations of V_d and RH were observed over wheat and maize canopy in the NCP (Zhu et al., 2014; Zhu et al., 2015), while O_3 deposition into a boreal forest revealed strong positive correlation with RH (Rannik et al., 2012), which was attributed to differences in plant varieties and growth environment. The response of stomata to the changes in humidity is largely dependent on plant cultivars and plant water stress (Camacho et al., 1974; Rawson et al., 1977; Fanourakis et al., 2020). For example, the stomata of drought-tolerant wheat cultivar closed rapidly with reduced humidity, whereas high-yield cultivar stomatal conductance increased against decreasing humidity (Kudoyarova et al., 2007). The growth environment affects the aerodynamically roughness of the earth surfaces. Increased roughness could induce stronger turbulent transfer under low humidity condition, transporting gases more effectively to the leaf surfaces, thereby promoting O_3 deposition (Liao et al., 2022).

Strong turbulence (represented by elevated u_*) can transport O_3 more efficiently to the surface (Cape et al., 2009), thus V_d almost linearly increased with u_* (Figure 7b and 9d). The sensitivity of V_d to u_* was also affected by LAI, with daytime V_d under similar levels of u_* being significantly higher under higher LAI (Figure 8a and Table S3). High LAI indicates dense vegetation coverage and potential large stomatal conductance, which can provide more active (stomatal and cuticular) areas for the uptake of O_3, further promoting O_3 deposition. PAR had a positive effect on O_3 deposition during the observation period (Figure 7c). On the one side, increasing PAR induces automatic leaf stomatal opening thereby determining stomatal conductance and net photosynthesis (Yu et al., 2004), affecting the stomatal O_3 uptake (Tong et al., 2015). On the other side, PAR (also reflecting radiation intensity) affects O_3 photochemistry directly by accelerating atmospheric photolysis reactions both above and within the canopy and indirectly by influencing the emission of biogenic VOCs (Yang et al., 2021; Van Meeningen et al., 2017; Yuan et al., 2016), thus disturbing the distributions of O_3 and its precursors and contributing non-stomatal O_3 fluxes with surface processes (Fares et al., 2008; Cape et al., 2009). Positive dependences of V_d on u_* and PAR were observed over other crop fields (such as wheat, maize, and potato) (Coyle et al., 2009; Zhu et al., 2014; Zhu et al., 2015). In addition, both T_{Air} and T_{Soil} exhibited weak relationships with nighttime V_d (Figures 9a, e), which were different from the reported positive correlations between temperature and V_d (Coyle et al., 2009; Rannik et al., 2012). These imply the variability and complexity of O_3 deposition affected by the combined influences of various environmental factors.

During the O-W and R-H stage, soil VWC was at relatively lower levels. During the G-F stage, soil VWC reached beyond 0.30% and V_d rose significantly with rising soil VWC (Figure 7d and 9f). Although soil moisture blocks the diffusion of O_3 in soil and reduces reactive spaces for O_3 absorption, suppressing O_3 soil deposition (Stella et al., 2011b), it can also promote total O_3 deposition through several indirect pathways. From the plant physiological aspect, stomatal conductance and plant net photosynthesis are both promoted by higher soil VWC (Otu-Larbi et al., 2021; Anav et al., 2018; Medlyn et al., 2011; Jarvis et al., 1997; Ball et al., 1987). Stomatal conductance revealed overshoots after the watering of dry soil, accordingly, significantly increased transpiration and photosynthesis of crops or vegetation were detected (Wu et al., 2021; Reich et al., 2018; Ramírez et al., 2018; Rawson and Clarke, 1988; Popescu, 1967). This effect was reflected at GC by the more obvious response of V_d to soil VWC changes under higher LAI (Figure 8b and Table S3), confirming again that O_3 deposition during

the G-F stage was mainly driven by stomatal deposition, rather than soil deposition. Consequently, soil VWC revealed positive coefficients in the MLR models for the G-F period at GC. Our result is qualitatively consistent with the observation based estimation of stomatal and soil O_3 deposition relative contributions over a wheat canopy in Nanjing city, China, which accounted for 41.2% and 15.4%, respectively (Xu et al., 2018).
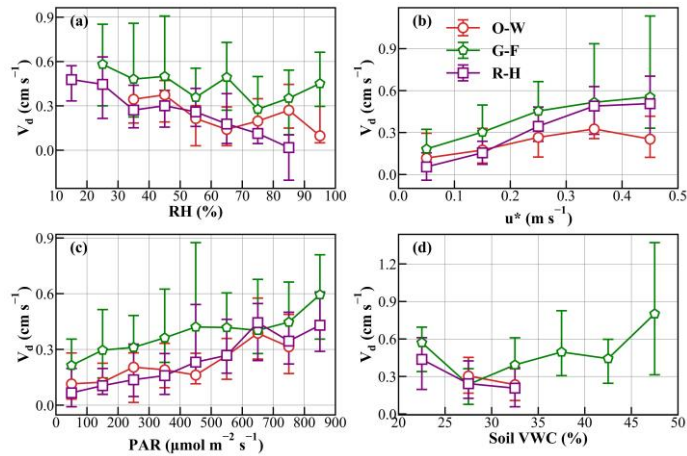
Figure 7. Dependences of daytime O_3 V_d on (a) RH, (b) u∗, (c) PAR and (d) soil VWC during the O-W, G-F and R-H stages. Medians of 30-min V_d with quartiles are presented.
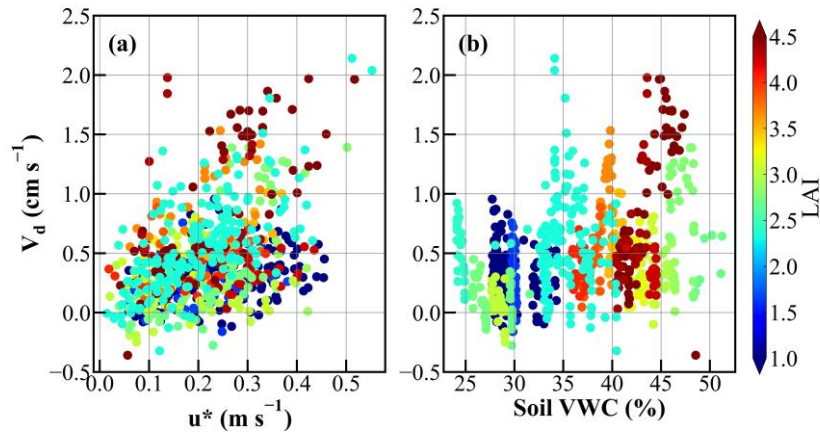
Figure 8. The variation of daytime V_d with (a) u∗, (b) soil VWC under changing LAI during the G-F stage.
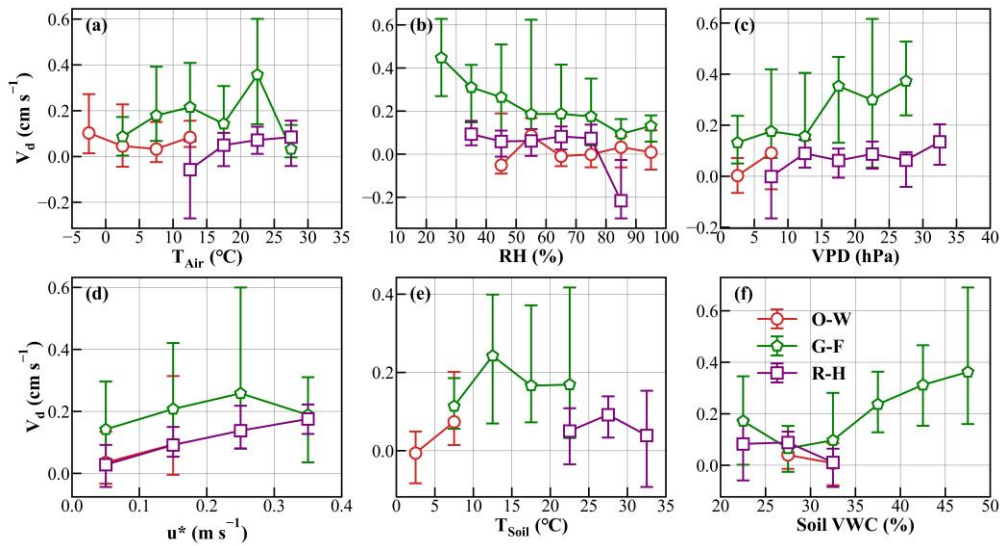
Figure 9. Dependences of O_3 V_d on (a) T_{Air}, (b) RH, (c) VPD, (d) u_*, (e) T_{Soil} and (f) soil VWC in the nighttime during the O-W, G-F and R-H stages. Medians of 30-min V_d with quartiles are presented.

Overall, soil VWC at GC kept low expect for four abrupt increasing events that occurred during the G-F stage, with the highest soil VWC reaching 0.55% (Figure 2c). The three most prominent episodes induced by farm field irrigation were more thoroughly investigated to uncover how soil moisture affected O_3 deposition at GC. Interestingly, simultaneous increments in V_d were detected upon the increase of soil VWC, with V_d being distinctly elevated within days afterwards (Figure 10). Soil VWC increased from 0.32% to 0.51% at noontime on 9 April, and V_d rapidly rose from 0.16 to 0.64 cm s^{-1} at the same time. Dramatic increments in both averaged nighttime and daytime V_d were detected on the following days. During nighttime, V_d reached an average of 0.30 cm s^{-1}, significantly higher than the average daytime level (0.18 cm s^{-1}) on 9 April, and a maximum of 0.76 cm s^{-1}, which also exceeded the maximum of 0.64 cm s^{-1} observed during the daytime of 9 April (Figure 10a). The dramatic rise in V_d on 10 April resulted a 317% increase in daytime O_3 deposition flux (from 0.12 µg m^{-2} s^{-1} to 0.50 µg m^{-2} s^{-1}), with only a small change in daytime O_3 concentration from 9 April (41.4 µg m^{-3}) to 10 April (48.2 µg m^{-3}, Figure S7a). In addition, drastic elevations in V_d during the night and morning periods were also observed following other episodes of sudden increases in soil VWC (Figure 10b, c). Similar enhancements and disrupted daily cycles of O_3 deposition were also observed over the canopy of a pine forest during rainfall events (Altimir et al., 2006).

Considering the direct effect of soil moisture on plant physiology, the temporal variations of CO_2 and H_2O fluxes were examined to characterize changes in transpiration and photosynthesis of wheat affected by the abrupt increases of soil water contents. As shown in Figure 11, both CO_2 and H_2O fluxes exhibited obvious increases on the days following the soil VWC increments. The daily peaks of H_2O fluxes increased from 0.08 to 0.13 g m^{-2} s^{-1} between 9 and 10 April and from 0.12 to 0.19 g m^{-2} s^{-1} between 28 and 29 April, respectively, while daily averaged CO_2 fluxes before and after the abrupt increasing events rose from 0.28 mg m^{-2} s^{-1} to 0.55 mg m^{-2} s^{-1} and 0.51 mg m^{-2} s^{-1} to 0.55 mg m^{-2} s^{-1}, respectively (Figure 11a, b). Subsequently,

CO_2 and H_2O fluxes, as well as V_d of O_3 exhibited declines with the slow loss in soil moisture (Figure 10 and 11). This indicates that transpiration and photosynthesis of wheat were sharply enhanced after soil water contents increased, leading to larger leaf stomatal conductance and strengthening O_3 stomatal uptake. These results were consistent with those obtained in previous conditional control experiments and field observations (Wu et al., 2021; Reich et al., 2018; Ramírez et al., 2018; Rawson and Clarke, 1988; Popescu, 1967). In addition, moist soil can extend the time window of wheat leaves' stomatal opening, both in the hours after sunset and before dawn (Schoppach et al., 2020; Ramírez et al., 2018). Stomata can even stay open during nighttime after precipitation or irrigation events (Kobayashi et al., 2007; Rawson and Clarke, 1988). During the irrigation induced high soil VWC episodes, positive H_2O fluxes were also observed at GC during the night, such as on 10 April and 28 April (Figure 11a, b), implying that wheat transpiration might not stop over the night and that leaf stomata might have not completely closed, continuing to uptake O_3 at night, significantly enhancing nocturnal O_3 deposition.

Additionally, the high nighttime O_3 deposition (V_d) phenomenon was always accompanied by positive water vapor fluxes and high NO concentrations, and occurred mainly after the rapid increase of soil VWC (Figure S8). As shown in Figure 10, high NO became more frequent at night during the high soil VWC events, and nighttime V_d dramatically increased when NO_x (NO and NO_2) fluctuated at obviously higher levels and nighttime O_3 concentration was still at low level (Figure S7), indicating a more intensive titration consumption of O_3 at night. This might be attributable to the fact that soil NO emissions were promoted by the watering process, as soil water content is a decisive factor for the transformation and emission of reactive nitrogen within soils (Schindlbacher et al., 2004; Ghude et al., 2010; Kim et al., 2012; Weber et al., 2015; Zörner et al., 2016). Enhanced nighttime soil NO emissions may inevitably cause stronger NO titration with O_3 within wheat canopy, facilitating the non-stomatal O_3 deposition at night.
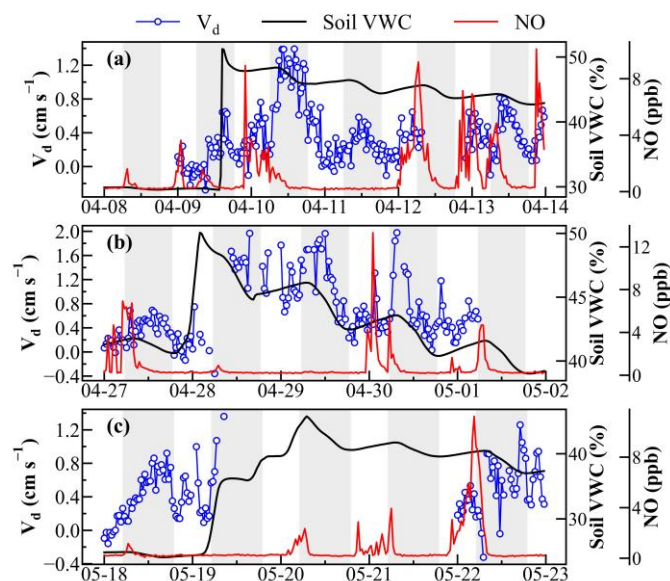
Figure 10. Variations of O_3 V_d (blue circle lines), soil VWC (black lines) and NO concentration (red lines) during (a) 8-13 April, (b) 27 April-1 May and (c) 18-22 May. The shades represent the daytime.
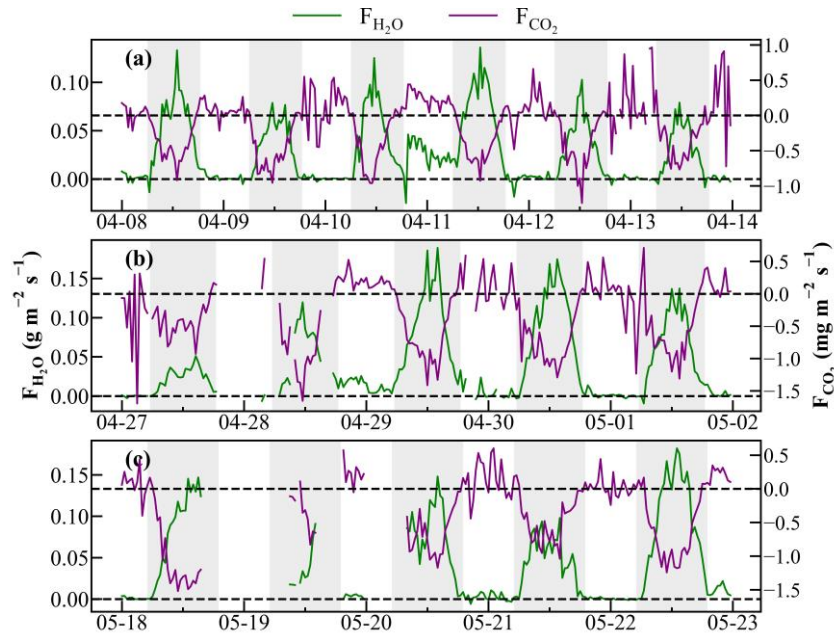
Figure 11. Variations of H₂O flux (F_{H_2O}, green lines) and CO₂ flux (F_{CO_2}, purple lines) during (a) 8-13 April, (b) 27 April-1 May and (c) 18-22 May, with shades representing daytime hours.

In summary, both daytime and nighttime O_3 deposition fluxes and V_d were significantly affected by environmental conditions, through stomatal and nonstomatal pathways, with crop growth playing a critical role. Abrupt increments in soil moisture induced dramatic changes in V_d, which not only altered the diurnal cycle of O_3 deposition, but also caused large fluctuations in averaged O_3 deposition flux on longer timescales.

4 Conclusions and implications

In this study, we developed a relaxed eddy accumulation (REA) O_3 flux measurement system, verified its reliability, and conducted measurements of O_3 deposition using this newly developed REA system over the wheat canopy at a polluted agricultural site (GC) in the NCP during the main wheat growth season. Ancillary data related to O_3 deposition and made an integrated analysis on the environmental influencing factors. The observed O_3 deposition flux and velocity over the wheat fields at GC reached averages of -0.25 ± 0.39 μg m^{-2} s^{-1} and 0.29 ± 0.33 cm s^{-1}, respectively. The diurnal cycle of V_d was controlled by the crop stomatal opening and turbulent transport during the day. V_d was obviously higher during daytime (0.40 ± 0.38 cm s^{-1}) than nighttime (0.17 ± 0.26 cm s^{-1}). V_d played a decisive role in the diel pattern of O_3 deposition flux, while O_3 concentrations determined the flux variability on longer timescales. The temporal changes of V_d were synchronous with the evolutions of LAI, wheat growth and cropland CO_2 flux, suggesting the determining and enhancement effect of crop growth

on O_3 deposition and the predominant contribution of stomatal uptake over wheat fields during its growth season. However, the relative contributions of stomatal and non-stomatal O_3 deposition pathways need to be further quantified in our future investigations, which is of crucial importance for studies on O_3 removal and vegetation health impacts. While the influence of crops on O_3 deposition through stomatal uptake or surface removal has been extensively investigated in previous studies (Ainsworth, 2017; Aunan et al., 2000; Bender and Weigel, 2011; Biswas et al., 2008; Epa, 2013; Felzer et al., 2005; Harmens et al., 2018; Piikki et al., 2008), those of O_3 deposition on crop growth and yield under currently rising O_3 levels in the NCP remains an unsolved issue. Many researches have assessed the crop yield loss induced by O_3 pollution based on exposure-response functions (Feng et al., 2019a; Hu et al., 2020; Feng et al., 2020). However, the actual exposure is more related to direct deposition flux measurements rather than concentration-based indicators (Zhu et al., 2015). Therefore, agricultural impacts of O_3 should be more accurately quantified using stomatal O_3 deposition fluxes that might be obtained from current total O_3 deposition flux measurements using partitioning methods such as those in Fares et al. (2013) in our following studies.

During the wheat growth season, RH, u_*, soil VWC and LAI were identified as the most significant factors in explaining the changes of O_3 deposition during daytime through stomatal and non-stomatal pathways, while u_* and soil VWC were more important for nocturnal O_3 deposition, which mainly commenced through non-stomatal deposition. V_d significantly increased with the decrease of RH and the increases of u_*, PAR and soil VWC, especially under higher LAI. Rapid increases of soil VWC after strong precipitation or irrigation events extended stomatal opening to nighttime hours, leading to increased stomatal conductance, enhanced transpiration and photosynthesis of wheat, which remarkably strengthened O_3 stomatal uptake during daytime and nighttime. Stomatal opening and transpiration are typically assumed to occur specifically during daytime. However, an increasing number of studies have shown the non-negligible effects of unclosed nocturnal stomata and transpiration for a wide range of plant species (Kukal and Irmak, 2022; Schoppach et al., 2020; Tamang et al., 2019; Ramírez et al., 2018; Hoshika et al., 2018). Therefore, how nocturnal plant activities would interact with the significantly increasing nighttime O_3 levels in China during recent years (Agathokleous et al., 2023; He et al., 2022) is also worth deeper investigations. Aside from influencing stomata opening, drastic changes in soil humidity also strengthened NO soil emissions, facilitating NO titration of O_3 within the canopy and enhancing non-stomatal O_3 removals at night. Therefore, drastically increasing soil moisture simultaneously led to strong increments in V_d. Under current climate warming trends, extreme weather events (such as extreme precipitation and drought) have gained in frequency in agricultural areas (Yuan et al., 2016), and its effect on agriculture, NO_x emissions, O_3 formation as well as O_3 deposition require future attentions.

During the entire wheat growth season, O_3 deposition velocity exhibited large fluctuations under changing environmental conditions, with distinct factors determining V_d variability during different wheat growth stages. These key influencing factors and their effects on O_3 deposition would also vary with canopy types and ground surface conditions. Aside from environmental conditions, agricultural activities also significantly affect O_3 deposition (Mészáros et al., 2009). Therefore, the actual O_3 deposition process bears large uncertainties and varies greatly in space and time. More O_3 deposition observations over different types of land surfaces and vegetations are urgently needed to facilitate the exploration on O_3 dry deposition

470 mechanisms and to optimize current model parameterizations whose results largely deviate from observed O_3 dry deposition fluxes in crop growth seasons (Clifton et al., 2020b; Hardacre et al., 2015).

Data availability

The data used in this study are available in the supplement data and can be made available from the corresponding authors
475 upon request.

Author contributions

XY and WX designed the experiment and XB led the research. XY made the O_3 deposition measurement with the help of WL, WX, ZG, XB and JM. JJ, ZL, SX, HR and GS were responsible for the EC flux measurement. XY analyzed the data and wrote the paper with help of WL, WX, XB.

480 ## Competing interest

The authors have no competing interests to declare.

Acknowledgments

This work is supported by the National Natural Science Foundation of China (42175127 and 41875159), Beijing Natural Science Foundation (8222078), CAMS projects (2023Z012 and 2020KJ003).

485 ## References

Agathokleous, E., Feng, Z., and Sicard, P.: Surge in nocturnal ozone pollution, Science, 382, 1131-1131, 10.1126/science.adm7628, 2023.
Ainsworth, E. A.: Understanding and improving global crop response to ozone pollution, The Plant Journal, 90, 886-897, https://doi.org/10.1111/tpj.13298, 2017.
Altimir, N., Kolari, P., Tuovinen, J. P., Vesala, T., Bäck, J., Suni, T., Kulmala, M., and Hari, P.: Foliage surface ozone deposition: a role for
490 surface moisture?, Biogeosciences, 3, 209-228, 10.5194/bg-3-209-2006, 2006.
Anav, A., Proietti, C., Menut, L., Carnicelli, S., De Marco, A., and Paoletti, E.: Sensitivity of stomatal conductance to soil moisture: implications for tropospheric ozone, Atmos. Chem. Phys., 18, 5747-5763, 10.5194/acp-18-5747-2018, 2018.
Aunan, K., Berntsen, T., and Seip, H.: Surface Ozone in China and its Possible Impact on Agricultural Crop Yields, Ambio, 29, 10.1639/0044-7447(2000)029[0294:SOICAI]2.0.CO;2, 2000.
495 Ball, J. T., Woodrow, I. E., and Berry, J. A.: A Model Predicting Stomatal Conductance and its Contribution to the Control of Photosynthesis under Different Environmental Conditions, in: Progress in Photosynthesis Research: Volume 4 Proceedings of the VIIth International Congress on Photosynthesis Providence, Rhode Island, USA, August 10–15, 1986, edited by: Biggins, J., Springer Netherlands, Dordrecht, 221-224, 10.1007/978-94-017-0519-6_48, 1987.
Bender, J. and Weigel, H.-J.: Changes in atmospheric chemistry and crop health: A review, Agronomy for Sustainable Development, 31, 81,
500 10.1051/agro/2010013, 2011.

Biswas, D. K., Xu, H., Li, Y. G., Sun, J. Z., Wang, X. Z., Han, X. G., and Jiang, G. M.: Genotypic differences in leaf biochemical, physiological and growth responses to ozone in 20 winter wheat cultivars released over the past 60 years, Global Change Biology, 14, 46-59, https://doi.org/10.1111/j.1365-2486.2007.01477.x, 2008.

Bowling, D. R., Delany, A. C., Turnipseed, A. A., Baldocchi, D. D., and Monson, R. K.: Modification of the relaxed eddy accumulation technique to maximize measured scalar mixing ratio differences in updrafts and downdrafts, J. Geophys. Res. Atmos., 104, 9121-9133, https://doi.org/10.1029/1999JD900013, 1999.

Businger, J. A. and Oncley, S. P.: Flux Measurement with Conditional Sampling, Journal of Atmospheric and Oceanic Technology, 7, 349-352, 10.1175/1520-0426(1990)007<0349:FMWCS>2.0.CO;2, 1990.

Camacho, B. S., Hall, A. E., and Kaufmann, M. R.: Efficiency and regulation of water transport in some woody and herbaceous species, Plant Physiol, 54, 169-172, 10.1104/pp.54.2.169, 1974.

Cape, J. N., Hamilton, R., and Heal, M. R.: Reactive uptake of ozone at simulated leaf surfaces: Implications for 'non-stomatal' ozone flux, Atmos. Environ., 43, 1116-1123, https://doi.org/10.1016/j.atmosenv.2008.11.007, 2009.

Clifton, O. E., Paulot, F., Fiore, A. M., Horowitz, L. W., Correa, G., Baublitz, C. B., Fares, S., Goded, I., Goldstein, A. H., Gruening, C., Hogg, A. J., Loubet, B., Mammarella, I., Munger, J. W., Neil, L., Stella, P., Uddling, J., Vesala, T., and Weng, E.: Influence of Dynamic Ozone Dry Deposition on Ozone Pollution, J. Geophys. Res. Atmos., 125, e2020JD032398, https://doi.org/10.1029/2020JD032398, 2020a.

Clifton, O. E., Fiore, A. M., Massman, W. J., Baublitz, C. B., Coyle, M., Emberson, L., Fares, S., Farmer, D. K., Gentine, P., Gerosa, G., Guenther, A. B., Helmig, D., Lombardozzi, D. L., Munger, J. W., Patton, E. G., Pusede, S. E., Schwede, D. B., Silva, S. J., Sörgel, M., Steiner, A. L., and Tai, A. P. K.: Dry Deposition of Ozone Over Land: Processes, Measurement, and Modeling, Reviews of Geophysics, 58, e2019RG000670, https://doi.org/10.1029/2019RG000670, 2020b.

Coyle, M.: The gaseous exchange of ozone at terrestrial surfaces : non-stomatal deposition to grassland,

Coyle, M., Nemitz, E., Storeton-West, R., Fowler, D., and Cape, J. N.: Measurements of ozone deposition to a potato canopy, Agricultural and Forest Meteorology, 149, 655-666, https://doi.org/10.1016/j.agrformet.2008.10.020, 2009.

Desjardins, R. L.: Description and evaluation of a sensible heat flux detector, Boundary-Layer Meteorology, 11, 147-154, 10.1007/BF02166801, 1977.

Dong, C., Gao, R., Zhang, X., Li, H., Wang, W., and Xue, L.: Assessment of O3-induced crop yield losses in northern China during 2013–2018 using high-resolution air quality reanalysis data, Atmos. Environ., 259, 118527, https://doi.org/10.1016/j.atmosenv.2021.118527, 2021.

EPA: Integrated Science Assessment (ISA) for Ozone and Related Photochemical Oxidants (Final Report, Feb 2013), Environmental Protection Agency, Washington, DC, U.S.2013.

Fanourakis, D., Aliniaeifard, S., Sellin, A., Giday, H., Körner, O., Rezaei Nejad, A., Delis, C., Bouranis, D., Koubouris, G., Kambourakis, E., Nikoloudakis, N., and Tsaniklidis, G.: Stomatal behavior following mid- or long-term exposure to high relative air humidity: A review, Plant Physiology and Biochemistry, 153, 92-105, https://doi.org/10.1016/j.plaphy.2020.05.024, 2020.

Fares, S., Loreto, F., Kleist, E., and Wildt, J.: Stomatal uptake and stomatal deposition of ozone in isoprene and monoterpene emitting plants, Plant Biology, 10, 44-54, https://doi.org/10.1055/s-2007-965257, 2008.

Fares, S., Matteucci, G., Scarascia Mugnozza, G., Morani, A., Calfapietra, C., Salvatori, E., Fusaro, L., Manes, F., and Loreto, F.: Testing of models of stomatal ozone fluxes with field measurements in a mixed Mediterranean forest, Atmos. Environ., 67, 242-251, https://doi.org/10.1016/j.atmosenv.2012.11.007, 2013.

Felzer, B., Reilly, J., Melillo, J., Kicklighter, D., Sarofim, M., Wang, C., Prinn, R., and Zhuang, Q.: Future Effects of Ozone on Carbon Sequestration and Climate Change Policy Using a Global Biogeochemical Model, Climatic Change, 73, 345-373, 10.1007/s10584-005-6776-4, 2005.

Feng, Z., Hu, T., Tai, A. P. K., and Calatayud, V.: Yield and economic losses in maize caused by ambient ozone in the North China Plain (2014–2017), Sci.Total Environ., 722, 137958, https://doi.org/10.1016/j.scitotenv.2020.137958, 2020.

Feng, Z., Kobayashi, K., Li, P., Xu, Y., Tang, H., Guo, A., Paoletti, E., and Calatayud, V.: Impacts of current ozone pollution on wheat yield in China as estimated with observed ozone, meteorology and day of flowering, Atmos. Environ., 217, 116945, https://doi.org/10.1016/j.atmosenv.2019.116945, 2019a.

Feng, Z., De Marco, A., Anav, A., Gualtieri, M., Sicard, P., Tian, H., Fornasier, F., Tao, F., Guo, A., and Paoletti, E.: Economic losses due to ozone impacts on human health, forest productivity and crop yield across China, Environ. Int., 131, 104966, https://doi.org/10.1016/j.envint.2019.104966, 2019b.

Fowler, D., Flechard, C., Cape, J. N., Storeton-West, R. L., and Coyle, M.: Measurements of Ozone Deposition to Vegetation Quantifying the Flux, the Stomatal and Non-Stomatal Components, Water, Air, and Soil Pollution, 130, 63-74, 10.1023/A:1012243317471, 2001.

Fu, Y. and Tai, A. P. K.: Impact of climate and land cover changes on tropospheric ozone air quality and public health in East Asia between 1980 and 2010, Atmos. Chem. Phys., 15, 10093-10106, 10.5194/acp-15-10093-2015, 2015.

Ghude, S. D., Lal, D. M., Beig, G., van der A, R., and Sable, D.: Rain-Induced Soil NOx Emission From India During the Onset of the Summer Monsoon: A Satellite Perspective, J. Geophys. Res. Atmos., 115, https://doi.org/10.1029/2009JD013367, 2010.

Grelle, A. and Keck, H.: Affordable relaxed eddy accumulation system to measure fluxes of H2O, CO2, CH4 and N2O from ecosystems, Agricultural and Forest Meteorology, 307, 108514, https://doi.org/10.1016/j.agrformet.2021.108514, 2021.

Han, H., Liu, J., Shu, L., Wang, T., and Yuan, H.: Local and synoptic meteorological influences on daily variability in summertime surface ozone in eastern China, Atmospheric Chemistry Physics, 20, 203-222, 10.5194/acp-20-203-2020, 2020.

Hardacre, C., Wild, O., and Emberson, L.: An evaluation of ozone dry deposition in global scale chemistry climate models, Atmos. Chem. Phys., 15, 6419-6436, 10.5194/acp-15-6419-2015, 2015.

560 Harmens, H., Hayes, F., Mills, G., Sharps, K., Osborne, S., and Pleijel, H.: Wheat yield responses to stomatal uptake of ozone: Peak vs rising background ozone conditions, Atmos. Environ., 173, 1-5, https://doi.org/10.1016/j.atmosenv.2017.10.059, 2018.

He, C., Lu, X., Wang, H., Wang, H., Li, Y., He, G., He, Y., Wang, Y., Zhang, Y., Liu, Y., Fan, Q., and Fan, S.: The unexpected high frequency of nocturnal surface ozone enhancement events over China: characteristics and mechanisms, Atmos. Chem. Phys., 22, 15243-15261, 10.5194/acp-22-15243-2022, 2022.

565 Held, A., Patton, E., Rizzo, L., Smith, J., Turnipseed, A., and Guenther, A.: Relaxed Eddy Accumulation Simulations of Aerosol Number Fluxes and Potential Proxy Scalars, Boundary-Layer Meteorology, 129, 451-468, 10.1007/s10546-008-9327-5, 2008.

Helmig, D., Lang, E. K., Bariteau, L., Boylan, P., Fairall, C. W., Ganzeveld, L., Hare, J. E., Hueber, J., and Pallandt, M.: Atmosphere-ocean ozone fluxes during the TexAQS 2006, STRATUS 2006, GOMECC 2007, GasEx 2008, and AMMA 2008 cruises, J. Geophys. Res. Atmos., 117, https://doi.org/10.1029/2011JD015955, 2012.

570 Hicks, B. B. and Wesely, M. L.: An examination of some micrometeorological methods for measuring dry deposition, EPA Interagency Energy/Environment R&D Program Report, a, EPA-600/607-678-116, 1978.

Hoshika, Y., Osada, Y., de Marco, A., Peñuelas, J., and Paoletti, E.: Global diurnal and nocturnal parameters of stomatal conductance in woody plants and major crops, Global Ecology and Biogeography, 27, 257-275, https://doi.org/10.1111/geb.12681, 2018.

Hu, T., Liu, S., Xu, Y., Feng, Z., and Calatayud, V.: Assessment of O3-induced yield and economic losses for wheat in the North China 575 Plain from 2014 to 2017, China, Environ. Pollut., 258, 113828, https://doi.org/10.1016/j.envpol.2019.113828, 2020.

Jarvis, P. G., Monteith, J. L., and Weatherley, P. E.: The interpretation of the variations in leaf water potential and stomatal conductance found in canopies in the field, Philosophical Transactions of the Royal Society of London. B, Biological Sciences, 273, 593-610, 10.1098/rstb.1976.0035, 1997.

Kim, D. G., Vargas, R., Bond-Lamberty, B., and Turetsky, M. R.: Effects of soil rewetting and thawing on soil gas fluxes: a review of current 580 literature and suggestions for future research, Biogeosciences, 9, 2459-2483, 10.5194/bg-9-2459-2012, 2012.

Kobayashi, N., Hiyama, T., Fukushima, Y., Lopez, M. L., Hirano, T., and Fujinuma, Y.: Nighttime transpiration observed over a larch forest in Hokkaido, Japan, Water Resources Research, 43, https://doi.org/10.1029/2006WR005556, 2007.

Kuang, Y., Xu, W., Lin, W., Meng, Z., Zhao, H., Ren, S., Zhang, G., Liang, L., and Xu, X.: Explosive morning growth phenomena of NH3 on the North China Plain: Causes and potential impacts on aerosol formation, Environ. Pollut., 257, 113621, 585 https://doi.org/10.1016/j.envpol.2019.113621, 2020.

Kudoyarova, G. R., Veselov, D. S., Faizov, R. G., Veselova, S. V., Ivanov, E. A., and Farkhutdinov, R. G.: Stomata response to changes in temperature and humidity in wheat cultivars grown under contrasting climatic conditions, Russian Journal of Plant Physiology, 54, 46-49, 10.1134/S1021443707010074, 2007.

Kukal, M. S. and Irmak, S.: Nocturnal transpiration in field crops: Implications for temporal aggregation and diurnal weighing of vapor 590 pressure deficit, Agricultural Water Management, 266, 107578, https://doi.org/10.1016/j.agwat.2022.107578, 2022.

Lamaud, E., Loubet, B., Irvine, M., Stella, P., Personne, E., and Cellier, P.: Partitioning of ozone deposition over a developed maize crop between stomatal and non-stomatal uptakes, using eddy-covariance flux measurements and modelling, Agricultural and Forest Meteorology, 149, 1385-1396, https://doi.org/10.1016/j.agrformet.2009.03.017, 2009.

Lelieveld, J. and Dentener, F. J.: What controls tropospheric ozone?, J. Geophys. Res. Atmos., 105, 3531-3551, 10.1029/1999JD901011, 595 2000.

Li, K., Jacob, D. J., Liao, H., Shen, L., Zhang, Q., and Bates, K. H.: Anthropogenic drivers of 2013–2017 trends in summer surface ozone in China, P. Natl. Acad. Sci., 116, 422, 10.1073/pnas.1812168116, 2019.

Liao, Q., Ding, R., Du, T., Kang, S., Tong, L., and Li, S.: Stomatal conductance drives variations of yield and water use of maize under water and nitrogen stress, Agricultural Water Management, 268, 107651, https://doi.org/10.1016/j.agwat.2022.107651, 2022.

600 Lin, W., Xu, X., Ge, B., and Zhang, X.: Characteristics of gaseous pollutants at Gucheng, a rural site southwest of Beijing, J. Geophys. Res. Atmos., 114, https://doi.org/10.1029/2008JD010339, 2009.

Lu, X., Zhang, L., Wang, X., Gao, M., Li, K., Zhang, Y., Yue, X., and Zhang, Y.: Rapid Increases in Warm-Season Surface Ozone and Resulting Health Impact in China Since 2013, Environmental Science & Technology Letters, 7, 240-247, https://doi.org/10.1021/acs.estlett.0c00171, 2020.

605 Lyu, X., Li, K., Guo, H., Morawska, L., Zhou, B., Zeren, Y., Jiang, F., Chen, C., Goldstein, A. H., Xu, X., Wang, T., Lu, X., Zhu, T., Querol, X., Chatani, S., Latif, M. T., Schuch, D., Sinha, V., Kumar, P., Mullins, B., Seguel, R., Shao, M., Xue, L., Wang, N., Chen, J., Gao, J., Chai, F., Simpson, I., Sinha, B., and Blake, D. R.: A synergistic ozone-climate control to address emerging ozone pollution challenges, One Earth, 6, 964-977, https://doi.org/10.1016/j.oneear.2023.07.004, 2023.

Ma, Z., Xu, J., Quan, W., Zhang, Z., Lin, W., and Xu, X.: Significant increase of surface ozone at a rural site, north of eastern China, Atmos. 610 Chem. Phys., 16, 3969-3977, 10.5194/acp-16-3969-2016, 2016.

Matsuda, K., Watanabe, I., Mizukami, K., Ban, S., and Takahashi, A.: Dry deposition of PM2.5 sulfate above a hilly forest using relaxed eddy accumulation, Atmos. Environ., 107, 255-261, 10.1016/j.atmosenv.2015.02.050, 2015.

Medlyn, B. E., Duursma, R. A., Eamus, D., Ellsworth, D. S., Prentice, I. C., Barton, C. V. M., Crous, K. Y., De Angelis, P., Freeman, M., and Wingate, L.: Reconciling the optimal and empirical approaches to modelling stomatal conductance, Global Change Biology, 17, 2134-2144, https://doi.org/10.1111/j.1365-2486.2010.02375.x, 2011.

Mészáros, R., Horváth, L., Weidinger, T., Neftel, A., Nemitz, E., Dämmgen, U., Cellier, P., and Loubet, B.: Measurement and modelling ozone fluxes over a cut and fertilized grassland, Biogeosciences, 6, 1987-1999, 10.5194/bg-6-1987-2009, 2009.

Mills, G., Pleijel, H., Malley, C. S., Sinha, B., Cooper, O. R., Schultz, M. G., Neufeld, H. S., Simpson, D., Sharps, K., Feng, Z., Gerosa, G., Harmens, H., Kobayashi, K., Saxena, P., Paoletti, E., Sinha, V., and Xu, X.: Tropospheric Ozone Assessment Report: Present-day tropospheric ozone distribution and trends relevant to vegetation, Elementa: Science of the Anthropocene, 6, 10.1525/elementa.302, 2018.

Mochizuki, T., Tani, A., Takahashi, Y., Saigusa, N., and Ueyama, M.: Long-term measurement of terpenoid flux above a Larix kaempferi forest using a relaxed eddy accumulation method, Atmos. Environ., 83, 53-61, 10.1016/j.atmosenv.2013.10.054, 2014.

Monks, P. S., Archibald, A. T., Colette, A., Cooper, O., Coyle, M., Derwent, R., Fowler, D., Granier, C., Law, K. S., Mills, G. E., Stevenson, D. S., Tarasova, O., Thouret, V., von Schneidemesser, E., Sommariva, R., Wild, O., and Williams, M. L.: Tropospheric ozone and its precursors from the urban to the global scale from air quality to short-lived climate forcer, Atmos. Chem. Phys., 15, 8889-8973, 10.5194/acp-15-8889-2015, 2015.

Moravek, A., Foken, T., and Trebs, I.: Application of a GC-ECD for measurements of biosphere–atmosphere exchange fluxes of peroxyacetyl nitrate using the relaxed eddy accumulation and gradient method, Atmos. Meas. Tech., 7, 2097-2119, 10.5194/amt-7-2097-2014, 2014.

Muller, J. B. A., Coyle, M., Fowler, D., Gallagher, M. W., Nemitz, E. G., and Percival, C. J.: Comparison of ozone fluxes over grassland by gradient and eddy covariance technique, Atmospheric Science Letters, 10, 164-169, https://doi.org/10.1002/asl.226, 2009.

Myneni, R., Knyazikhin, Y., and Park, T.: MCD15A3H MODIS/Terra+Aqua Leaf Area Index/FPAR 4-day L4 Global 500m SIN Grid V006 [dataset], https://doi.org/10.5067/MODIS/MCD15A3H.006, 2015.

Nelson, A. J., Koloutsou-Vakakis, S., Rood, M. J., Myles, L., Lehmann, C., Bernacchi, C., Balasubramanian, S., Joo, E., Heuer, M., Vieira-Filho, M., and Lin, J.: Season-long ammonia flux measurements above fertilized corn in central Illinois, USA, using relaxed eddy accumulation, Agricultural and Forest Meteorology, 239, 202-212, https://doi.org/10.1016/j.agrformet.2017.03.010, 2017.

Osterwalder, S., Fritsche, J., Alewell, C., Schmutz, M., Nilsson, M. B., Jocher, G., Sommar, J., Rinne, J., and Bishop, K.: A dual-inlet, single detector relaxed eddy accumulation system for long-term measurement of mercury flux, Atmos. Meas. Tech., 9, 509-524, 10.5194/amt-9-509-2016, 2016.

Otu-Larbi, F., Conte, A., Fares, S., Wild, O., and Ashworth, K.: FORCAsT-gs: Importance of Stomatal Conductance Parameterization to Estimated Ozone Deposition Velocity, 13, e2021MS002581, https://doi.org/10.1029/2021MS002581, 2021.

Pattey, E., Desjardins, R. L., and Rochette, P.: Accuracy of the relaxed eddy-accumulation technique, evaluated using CO2 flux measurements, Boundary-Layer Meteorology, 66, 341-355, 10.1007/BF00712728, 1993.

Piikki, K., De Temmerman, L., Ojanperä, K., Danielsson, H., and Pleijel, H.: The grain quality of spring wheat (Triticum aestivum L.) in relation to elevated ozone uptake and carbon dioxide exposure, European Journal of Agronomy, 28, 245-254, https://doi.org/10.1016/j.eja.2007.07.004, 2008.

Popescu, F.: Transpiration and the economic coefficient of transpiration of Bezostaya wheat as dependent on soil moisture content, Bul. stunt, Univ. Craiova., 9, 67-76, 1967.

Ramírez, D. A., Yactayo, W., Rolando, J. L., and Quiroz, R.: Preliminary Evidence of Nocturnal Transpiration and Stomatal Conductance in Potato and their Interaction with Drought and Yield, American Journal of Potato Research, 95, 139-143, 10.1007/s12230-017-9618-9, 2018.

Rannik, Ü., Altimir, N., Mammarella, I., Bäck, J., Rinne, J., Ruuskanen, T. M., Hari, P., Vesala, T., and Kulmala, M.: Ozone deposition into a boreal forest over a decade of observations: evaluating deposition partitioning and driving variables, Atmos. Chem. Phys., 12, 12165-12182, 10.5194/acp-12-12165-2012, 2012.

Raupach, M. R. and Thom, A. S.: Turbulence in and above Plant Canopies, Annual Review of Fluid Mechanics, 13, 97-129, 10.1146/annurev.fl.13.010181.000525, 1981.

Rawson, H. M. and Clarke, J. M.: Nocturnal transpiration in wheat, Australian Journal of Plant Physiology, 15, 397-406, 10.1071/pp9880397, 1988.

Rawson, H. M., Begg, J. E., and Woodward, R. G.: The effect of atmospheric humidity on photosynthesis, transpiration and water use efficiency of leaves of several plant species, Planta, 134, 5-10, 10.1007/BF00390086, 1977.

Reich, P. B., Sendall, K. M., Stefanski, A., Rich, R. L., Hobbie, S. E., and Montgomery, R. A.: Effects of climate warming on photosynthesis in boreal tree species depend on soil moisture, Nature, 562, 263-267, 10.1038/s41586-018-0582-4, 2018.

Ren, X., Sanders, J. E., Rajendran, A., Weber, R. J., Goldstein, A. H., Pusede, S. E., Browne, E. C., Min, K. E., and Cohen, R. C.: A relaxed eddy accumulation system for measuring vertical fluxes of nitrous acid, Atmos. Meas. Tech., 4, 2093-2103, 10.5194/amt-4-2093-2011, 2011.

665 Sarkar, C., Turnipseed, A., Shertz, S., Karl, T., Potosnak, M., Bai, J., Serça, D., Bonal, D., Burban, B., Lopes, P. R. C., Vega, O., and Guenther, A. B.: A portable, low-cost relaxed eddy accumulation (REA) system for quantifying ecosystem-level fluxes of volatile organics, Atmos. Environ., 242, 117764, https://doi.org/10.1016/j.atmosenv.2020.117764, 2020.

Schindlbacher, A., Zechmeister-Boltenstern, S., and Butterbach-Bahl, K.: Effects of soil moisture and temperature on NO, NO2, and N2O emissions from European forest soils, J. Geophys. Res. Atmos., 109, https://doi.org/10.1029/2004JD004590, 2004.

670 Schoppach, R., Sinclair, T. R., and Sadok, W.: Sleep tight and wake-up early: nocturnal transpiration traits to increase wheat drought tolerance in a Mediterranean environment, Funct Plant Biol, 47, 1117-1127, 10.1071/fp20044, 2020.

Seinfeld, J. H., Pandis, S. N., and Noone, K.: Atmospheric Chemistry and Physics: From Air Pollution to Climate Change, 2nd, John Wiley & Sons, Inc., Hoboken, New Jersey, United States2006.

Stella, P., Loubet, B., Lamaud, E., Laville, P., and Cellier, P.: Ozone deposition onto bare soil: A new parameterisation, Agricultural and 675 Forest Meteorology, 151, 669-681, https://doi.org/10.1016/j.agrformet.2011.01.015, 2011a.

Stella, P., Loubet, B., de Berranger, C., Charrier, X., Ceschia, E., Gerosa, G., Finco, A., Lamaud, E., Serça, D., George, C., and Ciuraru, R.: Soil ozone deposition: Dependence of soil resistance to soil texture, Atmos. Environ., 199, 202-209, 10.1016/j.atmosenv.2018.11.036, 2019.

Stella, P., Personne, E., Loubet, B., Lamaud, E., Ceschia, E., Béziat, P., Bonnefond, J. M., Irvine, M., Keravec, P., Mascher, N., and Cellier, P.: Predicting and partitioning ozone fluxes to maize crops from sowing to harvest: the Surfatm-O$_3$ model, Biogeosciences, 8, 680 2869-2886, 10.5194/bg-8-2869-2011, 2011b.

Stocker, D. W., Zeller, K. F., and Stedman, D. H.: O3 and NO2 fluxes over snow measured by eddy correlation, Atmos. Environ., 29, 1299-1305, https://doi.org/10.1016/1352-2310(94)00337-K, 1995.

Tai, A. P. K., Martin, M. V., and Heald, C. L.: Threat to future global food security from climate change and ozone air pollution, Nature Climate Change, 4, 817-821, 10.1038/nclimate2317, 2014.

685 Tamang, B. G., Schoppach, R., Monnens, D., Steffenson, B. J., Anderson, J. A., and Sadok, W.: Variability in temperature-independent transpiration responses to evaporative demand correlate with nighttime water use and its circadian control across diverse wheat populations, Planta, 250, 115-127, 10.1007/s00425-019-03151-0, 2019.

Tang, G., Zhu, X., Xin, J., Hu, B., Song, T., Sun, Y., Zhang, J., Wang, L., Cheng, M., Chao, N., Kong, L., Li, X., and Wang, Y.: Modelling study of boundary-layer ozone over northern China - Part I: Ozone budget in summer, Atmospheric Research, 187, 128-137, 690 https://doi.org/10.1016/j.atmosres.2016.10.017, 2017.

Tong, L., Xiao, H., Qian, F., Huang, Z., Feng, J., and Wang, X.: Daytime and Phenological Characteristics of O3 and CO2 Fluxes of Winter Wheat Canopy Under Short-Term O3 Exposure, Water, Air, & Soil Pollution, 227, 4, 10.1007/s11270-015-2698-6, 2015.

Tsai, J.-L., Tsuang, B.-J., Kuo, P.-H., Tu, C.-Y., Chen, C.-L., Hsueh, M.-T., Lee, C.-S., Yao, M.-H., and Hsueh, M.-L.: Evaluation of the relaxed eddy accumulation coefficient at various wetland ecosystems, Atmos. Environ., 60, 336-347, 10.1016/j.atmosenv.2012.06.081, 2012.

695 van Meeningen, Y., Schurgers, G., Rinnan, R., and Holst, T.: Isoprenoid emission response to changing light conditions of English oak, European beech and Norway spruce, Biogeosciences, 14, 4045-4060, 10.5194/bg-14-4045-2017, 2017.

Venables, W. N. and Ripley, B. D.: Modern Applied Statistics with S, Springer, NewYork, USA2003.

Vilà-Guerau De Arellano, J. and Duynkerke, P. G.: Influence of chemistry on the flux-gradient relationships for the NO-O3-NO2 system, Boundary-Layer Meteorology, 61, 375-387, 10.1007/BF00119098, 1992.

700 Wang, P., Yang, Y., Li, H., Chen, L., Dang, R., Xue, D., Li, B., Tang, J., Leung, L. R., and Liao, H.: North China Plain as a hot spot of ozone pollution exacerbated by extreme high temperatures, Atmos. Chem. Phys., 22, 4705-4719, 10.5194/acp-22-4705-2022, 2022.

Wang, T., Xue, L., Brimblecombe, P., Lam, Y. F., Li, L., and Zhang, L.: Ozone pollution in China: A review of concentrations, meteorological influences, chemical precursors, and effects, Sci.Total Environ., 575, 1582-1596, https://doi.org/10.1016/j.scitotenv.2016.10.081, 2017.

705 Weber, B., Wu, D., Tamm, A., Ruckteschler, N., Rodríguez-Caballero, E., Steinkamp, J., Meusel, H., Elbert, W., Behrendt, T., Sörgel, M., Cheng, Y., Crutzen, P. J., Su, H., and Pöschl, U.: Biological soil crusts accelerate the nitrogen cycle through large NO and HONO emissions in drylands, P. Natl. Acad. Sci., 112, 15384-15389, 10.1073/pnas.1515818112, 2015.

Wild, O.: Modelling the global tropospheric ozone budget: exploring the variability in current models, Atmos. Chem. Phys., 7, 2643-2660, 10.5194/acp-7-2643-2007, 2007.

710 Wu, X., Xu, Y., Shi, J., Zuo, Q., Zhang, T., Wang, L., Xue, X., and Ben-Gal, A.: Estimating stomatal conductance and evapotranspiration of winter wheat using a soil-plant water relations-based stress index, Agricultural and Forest Meteorology, 303, 108393, https://doi.org/10.1016/j.agrformet.2021.108393, 2021.

Wu, Z. Y., Zhang, L., Wang, X. M., and Munger, J. W.: A modified micrometeorological gradient method for estimating O$_3$ dry depositions over a forest canopy, Atmos. Chem. Phys., 15, 7487-7496, 10.5194/acp-15-7487-2015, 2015.

715 Xu, J., Zheng, Y., Mai, B., Zhao, H., Chu, Z., Huang, J., and Yuan, Y.: Simulating and partitioning ozone flux in winter wheat field: the Surfatm-O3 model (in Chinese), China Environmental Science 38, 455-470, 2018.

Xu, M., Kasahara, K., Sorimachi, A., and Matsuda, K.: Nitric acid dry deposition associated with equilibrium shift of ammonium nitrate above a forest by long-term measurement using relaxed eddy accumulation, Atmos. Environ., 256, 118454, https://doi.org/10.1016/j.atmosenv.2021.118454, 2021.

720 Xu, W., Kuang, Y., Zhao, C., Tao, J., Zhao, G., Bian, Y., Yang, W., Yu, Y., Shen, C., Liang, L., Zhang, G., Lin, W., and Xu, X.: NH3-promoted hydrolysis of NO2 induces explosive growth in HONO, Atmos. Chem. Phys., 19, 10557-10570, 10.5194/acp-19-10557-2019, 2019.

Xu, X.: Recent advances in studies of ozone pollution and impacts in China: A short review, Current Opinion in Environmental Science & Health, 19, 100225, https://doi.org/10.1016/j.coesh.2020.100225, 2021.

725 Xu, X., Bingemer, H. G., and Schmidt, U.: The flux of carbonyl sulfide and carbon disulfide between the atmosphere and a spruce forest, Atmos. Chem. Phys., 2, 171-181, 10.5194/acp-2-171-2002, 2002.

Xu, X., Lin, W., Xu, W., Jin, J., Wang, Y., Zhang, G., Zhang, X., Ma, Z., Dong, Y., Ma, Q., Yu, D., Li, Z., Wang, D., and Zhao, H.: Long-term changes of regional ozone in China: implications for human health and ecosystem impacts, Elementa: Science of the Anthropocene, 8, 10.1525/elementa.409, 2020.

730 Yang, W., Cao, J., Wu, Y., Kong, F., and Li, L.: Review on plant terpenoid emissions worldwide and in China, Sci.Total Environ., 787, 147454, https://doi.org/10.1016/j.scitotenv.2021.147454, 2021.

Yu, Q., Zhang, Y., Liu, Y., and Shi, P.: Simulation of the Stomatal Conductance of Winter Wheat in Response to Light, Temperature and CO2 Changes, Annals of Botany, 93, 435-441, 10.1093/aob/mch023 %J Annals of Botany, 2004.

Yuan, X., Calatayud, V., Gao, F., Fares, S., Paoletti, E., Tian, Y., and Feng, Z.: Interaction of drought and ozone exposure on isoprene 735 emission from extensively cultivated poplar, Plant, Cell & Environment, 39, 2276-2287, https://doi.org/10.1111/pce.12798, 2016.

Zhang, X., Xu, W., Zhang, G., Lin, W., Zhao, H., Ren, S., Zhou, G., Chen, J., and Xu, X.: Discrepancies in ozone levels and temporal variations between urban and rural North China Plain: Possible implications for agricultural impact assessment across China, Elementa: Science of the Anthropocene, 10, 10.1525/elementa.2022.00019, 2022a.

Zhang, X., Xu, W., Zhang, G., Lin, W., Zhao, H., Ren, S., Zhou, G., Chen, J., and Xu, X.: First long-term surface ozone variations at an 740 agricultural site in the North China Plain: Evolution under changing meteorology and emissions, Sci.Total Environ., 160520, https://doi.org/10.1016/j.scitotenv.2022.160520, 2022b.

Zhu, Z., Sun, X., Zhao, F., and Meixner, F. X.: Ozone concentrations, flux and potential effect on yield during wheat growth in the Northwest-Shandong Plain of China, Journal of Environmental Sciences, 34, 1-9, https://doi.org/10.1016/j.jes.2014.12.022, 2015.

Zhu, Z., Sun, X., Dong, Y., Zhao, F., and Meixner, F. X.: Diurnal variation of ozone flux over corn field in Northwestern Shandong Plain 745 of China, Science China Earth Sciences, 57, 503-511, 10.1007/s11430-013-4797-9, 2014.

Zörner, J., Penning de Vries, M., Beirle, S., Sihler, H., Veres, P. R., Williams, J., and Wagner, T.: Multi-satellite sensor study on precipitation-induced emission pulses of NOx from soils in semi-arid ecosystems, Atmos. Chem. Phys., 16, 9457-9487, 10.5194/acp-16-9457-2016, 2016.